

# Accuracy of Finite Element Approximations for Two-dimensional Time-harmonic Electromagnetic Boundary Value Problems Involving Non-conducting Moving Objects with Stationary Boundaries

**Praveen K. Ramakrishnan and Mirco Raffetto**

Department of Electrical Electronic, Telecommunications Engineering and Naval Architecture  
University of Genoa, Via Opera Pia 11a, 16145, Genoa, Italy  
pravin.nitc@gmail.com, raffetto@dibe.unige.it

**Abstract** — An analysis of the accuracy of the results computed using a finite element code in the presence of axially moving cylinders is presented. It seems that no result of this type is available in the open literature.

Any material in motion is perceived as a bianisotropic medium. This generates a scattered field having two components: one has the same polarization as the incident field and the other presents the orthogonal polarization. The results on the accuracy of the copolarized field are new but are similar to those obtained in the presence of motionless media. The outcome on the accuracy of the results related to the orthogonal polarization seems to be more interesting, especially for the information content this component of the field could provide on the axial velocity profile. In particular, using a finite element simulator based on double precision arithmetic, it is shown that the range of axial velocity values over which it is possible to obtain very accurate approximations can span nine or even more decades. This allows the use of the simulator, even when the more difficult components of the field are required to be accurate, for a set of applications ranging from astrophysics to medicine.

**Index Terms** — Bianisotropic media, electromagnetic scattering, error analysis, finite element method, moving media, reconstruction of velocity profiles, time-harmonic electromagnetic fields.

## I. INTRODUCTION

The interaction of electromagnetic waves with moving bodies plays a role in many applications [1], [2]. Among these, one can consider many important applications involving only axially moving cylinders. In particular, one can refer to axially moving plasma columns [3], [4], [5], ionized meteor trails [6], jet exhausts [7] or mass flow in pneumatic pipes [8].

In most cases of interest, which could involve multiple cylinders having irregular shapes, inhomogeneous constitutive parameters and non-constant velocity profiles,

numerical methods are required to try to approximate the solutions of interest [9].

Notwithstanding the difficulty related to the presence of materials in motion [1], [10], [11], determining the appearance of bianisotropic materials in any reference frame in which the media themselves are not at rest, the first results related to the well-posedness and the finite element approximability for these problems have been deduced [12].

When simulators are exploited, the results related to the convergence of numerical approximations are not the only aspects of practical interest. However, error estimates [13] are important too (particularly, a-priori error estimations), as clearly pointed out in [14] (p. 114). These estimations are not available so far, to the best of authors' knowledge, for two dimensional problems involving moving objects. In particular, results are not available for problems involving axially moving cylinders, like the ones of interest in this paper.

Then, in order to understand what can be expected in practice, we have to perform numerical experiments. Unfortunately, in the presence of axially moving cylinders, no numerical analysis seems to be available. This is the reason why, in this paper, we present a lot of numerical results. They could suggest what can be expected in other cases and could be considered as benchmarks for any error estimate the research community will be able to deduce.

All numerical results which will be presented refer to a simple problem involving a moving cylinder. For such a problem an independent truncated-series solution can be found [4] (see also [15]). In this way, we can evaluate the accuracy of our finite element approximations in terms of absolute and relative errors. The effects of all parameters involved in the definition of the simple problem of reference are studied.

As it has already been pointed out, in the presence of a time-harmonic illumination, the axial motion of cylinders determines, in any reference frame in which the media are not at rest, a bianisotropic effect and this,

in turn, is responsible for the presence of a scattered field having both polarizations: the same as that of the incident field and the orthogonal one. For the co-polarized component of the field the outcome is absolutely stable. The errors for this component are, in particular, almost independent of the axial velocity and, then, assume almost the same values we get in the presence of motionless media. For the cross-polarized scattered wave the relative errors are very stable, as well, even though it is a-priori known that the previous results cannot be duplicated in this case, due to the fact that this component of the scattered field is known to go uniformly to zero as the axial speed of the scatterers becomes smaller and smaller [16]. Anyway, the errors on this component of the scattered field are indeed stable for a huge range of axial velocity values. By using double precision arithmetic this range can span nine or even more decades, so allowing the use of finite element simulators for velocities varying from a few centimeters per second to many thousands of kilometers per second. That means that the considered finite element method can be reliably used for a set of applications ranging from astrophysics to medicine.

In the paper, we examine the behavior of the error in the co-polarized and cross-polarized components of the field. The results of numerical experiments indicate that the co-polarized component follows quadratic convergence, same as that in the motionless case. On the other hand, the results show that the cross-polarized component has linear convergence. However, at low values of axial speed we expect that the round-off error becomes more and more significant, degrading the accuracy of the cross-polarized component. This is because the co-polarized component remains of the same order of magnitude while the cross-polarized component goes to zero with decreasing velocity. When the ratio of the norm of the cross-polarized component to the co-polarized component becomes too large, the result becomes less reliable. Hence, this number can be used as a general indicator for checking if the results of the simulation are reliable or not.

The results show, in addition to the previously mentioned applications, that the indicated simulator can be exploited as a reliable solver of forward scattering problems in imaging procedures aiming at the reconstruction of axial velocity profiles [16], [17] and this, by the way, was the initial motivation for our study.

The paper is organized as follows. In Section II the mathematical formulation of the problems of interest is recalled together with some of the results available in the open literature. Some new considerations on the properties of the finite element matrices in the presence of moving media are provided in Section III. In order to carry out the error analysis of interest, the definition of a test case is necessary. This is done in Section IV,

where, in addition, a complete set of relevant absolute and relative errors is defined. The main section of the manuscript, dealing with the error analysis, is Section V. Finally, before concluding the paper, some considerations on the convergence of two well-known iterative methods are provided.

## II. MATHEMATICAL FORMULATION OF THE PROBLEM

The electromagnetic problems of interest in this paper are those in which axially moving cylinders (having parallel axes) are illuminated by a time-harmonic source or field. This class of problems has been studied in [12] and we refer to that paper for the definition of all details. Here we recall just the main points to let the readers understand the developments which will be presented in the next sections.

All our problems will present a cylindrical geometry and we denote by  $z$  the axis of such a geometry. The time-harmonic sources and the inhomogeneous admittance boundary conditions involved are assumed to be independent of  $z$ , too, so that our problems can be formulated in a two-dimensional domain  $\Omega$  contained in the  $(x, y)$  plane.  $\Gamma$  denotes the boundary of  $\Omega$ .  $\mathbf{n}$  and  $\mathbf{l}$  are the unit vectors orthogonal (pointing outward) and tangential to  $\Gamma$ , respectively. We have  $\mathbf{n} \times \mathbf{l} = \hat{\mathbf{z}}$ .

The media involved in our problems can move in the axial direction with respect to the chosen reference frame. In such a frame a velocity field  $v_z$ , assumed to be time-invariant, is naturally defined, even though we will often refer to it in terms of the usual [18] (p. 525) real-valued normalized field  $\beta = \frac{v_z}{c_0}$ , being  $c_0$  the speed of light in vacuum. Different linear, time-invariant and inhomogeneous materials can be modelled in our problems.  $\Omega_\beta$  will denote the subdomain of  $\Omega$  containing all media in motion.

Under the indicated conditions all fields in all media will be time-harmonic, as the considered sources, and a factor  $e^{j\omega t}$ , common to all fields of interest, is assumed and suppressed.

Any material involved is isotropic in its rest frame and is there characterized by its relative permittivity  $\epsilon_r$ , its relative permeability  $\mu_r$ , and its electric conductivity  $\sigma$ . In the following, any reference to  $\epsilon_r$ ,  $\mu_r$  or  $\sigma$  of a moving medium should be interpreted as a reference to the corresponding quantity when the medium is at rest. All moving media will be considered in any case to have  $\sigma = 0$  (in order to avoid the difficulties related to the convective currents which could also become surface electric currents and to avoid difficulty related to the no-slip condition which, ultimately, prevents the possibility of using pure two-dimensional models [12]).

By using the subscript “t” to denote the field quantities transverse to the  $z$  direction, the constitutive

relations for the media in motion are [12]:

$$\mathbf{D}_t = \frac{1 + \mu_r \varepsilon_r - \zeta_1}{c_0^2 \mu_0 \mu_r} \mathbf{E}_t + \frac{\zeta_2}{c_0 \mu_0 \mu_r} \hat{\mathbf{z}} \times \mathbf{B}_t, \quad (1)$$

$$D_z = \varepsilon_0 \varepsilon_r E_z, \quad (2)$$

$$\mathbf{H}_t = \frac{\zeta_1}{\mu_0 \mu_r} \mathbf{B}_t + \frac{\zeta_2}{c_0 \mu_0 \mu_r} \hat{\mathbf{z}} \times \mathbf{E}_t, \quad (3)$$

$$H_z = \frac{1}{\mu_0 \mu_r} B_z, \quad (4)$$

where

$$\zeta_1 = \frac{1 - \mu_r \varepsilon_r \beta^2}{1 - \beta^2}, \quad (5)$$

$$\zeta_2 = \frac{\beta(\mu_r \varepsilon_r - 1)}{1 - \beta^2}. \quad (6)$$

In order to be able to define the problems of interest and to talk of their finite element approximations, it is necessary to introduce some additional notations.  $(L^2(\Omega))^n$  is the usual Hilbert space of square integrable vector fields on  $\Omega$  with values in  $\mathbb{C}^n$ ,  $n = 2, 3$ , and with scalar product given by  $(\mathbf{u}, \mathbf{v})_{0,\Omega} = \int_{\Omega} \mathbf{v}^* \mathbf{u} \, dS$ , where  $\mathbf{v}^*$  denotes the conjugate transpose of the column vector  $\mathbf{v}$ . For a given three-dimensional complex-valued vector field  $\mathbf{A} = (A_x, A_y, A_z) \in (L^2(\Omega))^3$  we consider the operators  $\text{curl}_{2D}$  and  $\text{grad}_{2D}$ , defined according to:

$$\text{curl}_{2D} \mathbf{A}_t = \frac{\partial A_y}{\partial x} - \frac{\partial A_x}{\partial y}, \quad (7)$$

$$\text{grad}_{2D} A_z = \left( \frac{\partial A_z}{\partial x}, \frac{\partial A_z}{\partial y} \right). \quad (8)$$

The transverse parts of the electric and magnetic fields will be in the Hilbert space:

$$U_{2D} = \left\{ \mathbf{A}_t \in (L^2(\Omega))^2 \mid \text{curl}_{2D} A_t \in L^2(\Omega) \right. \\ \left. \text{and } \mathbf{A}_t \cdot \mathbf{l} \in L^2(\Gamma) \right\}, \quad (9)$$

whose inner product is given by:

$$(\mathbf{u}_t, \mathbf{v}_t)_{U_{2D}} = (\mathbf{u}_t, \mathbf{v}_t)_{0,\Omega} + (\text{curl}_{2D} \mathbf{u}_t, \text{curl}_{2D} \mathbf{v}_t)_{0,\Omega} \\ + (\mathbf{u}_t \cdot \mathbf{l}, \mathbf{v}_t \cdot \mathbf{l})_{0,\Gamma}. \quad (10)$$

The axial components of the same fields are in the Hilbert space:

$$H^1(\Omega) = \left\{ A_z \in L^2(\Omega) \mid \text{grad}_{2D} A_z \in (L^2(\Omega))^2 \right\}, \quad (11)$$

whose inner product is:

$$(u_z, v_z)_{1,\Omega} = (u_z, v_z)_{0,\Omega} + (\text{grad}_{2D} u_z, \text{grad}_{2D} v_z)_{0,\Omega}. \quad (12)$$

$\gamma_0 u_z$  will denote the boundary values of  $u_z \in H^1(\Omega)$  on  $\Gamma$ .

Overall the electric and magnetic fields are in the Hilbert space:

$$U = U_{2D} \times H^1(\Omega), \quad (13)$$

with inner product given by:

$$(\mathbf{u}, \mathbf{v})_U = (\mathbf{u}_t, \mathbf{v}_t)_{U_{2D}} + (u_z, v_z)_{1,\Omega}. \quad (14)$$

$\| \cdot \|_U$  will denote the corresponding norm. The norms of the different spaces so far introduced will be of particular

interest in establishing the accuracy of the results of the finite element simulator considered.

With the indicated notation, the electromagnetic boundary value problem we consider in this paper is: given  $\omega > 0$ , the electric and magnetic current densities  $\mathbf{J}_e, \mathbf{J}_m \in (L^2(\Omega))^3$ , the boundary data  $f_{Rz}, f_{Rl} \in L^2(\Gamma)$ , find  $(\mathbf{E}, \mathbf{B}, \mathbf{H}, \mathbf{D}) \in U \times (L^2(\Omega))^3 \times U \times (L^2(\Omega))^3$  which satisfies:

$$\begin{cases} \text{curl}_{2D} \mathbf{H}_t - j\omega \mathbf{D}_z = J_{ez} & \text{in } \Omega, \\ \text{grad}_{2D} H_z \times \hat{\mathbf{z}} - j\omega \mathbf{D}_t = \mathbf{J}_{et} & \text{in } \Omega, \\ \text{curl}_{2D} \mathbf{E}_t + j\omega \mathbf{B}_z = -\mathbf{J}_{mz} & \text{in } \Omega, \\ \text{grad}_{2D} E_z \times \hat{\mathbf{z}} + j\omega \mathbf{B}_t = -\mathbf{J}_{mt} & \text{in } \Omega, \\ \mathbf{H}_t \cdot \mathbf{l} + Y(\gamma_0 E_z) = -f_{Rz} & \text{on } \Gamma, \\ \gamma_0 H_z - Y(\mathbf{E}_t \cdot \mathbf{l}) = f_{Rl} & \text{on } \Gamma, \end{cases} \quad (15)$$

and the constitutive relations (1), (2), (3) and (4).

After some work [12], one can deduce the equivalent variational formulation: given  $\omega > 0$ ,  $\mathbf{J}_e, \mathbf{J}_m \in (L^2(\Omega))^3$ ,  $f_{Rz}, f_{Rl} \in L^2(\Gamma)$ , find  $\mathbf{E} \in U$  such that:

$$a(\mathbf{E}, \mathbf{w}) = l(\mathbf{w}) \quad \forall \mathbf{w} \in U, \quad (16)$$

where  $a$  is the following sesquilinear form:

$$\begin{aligned} a(\mathbf{u}, \mathbf{w}) = & \left( \frac{\zeta_1}{\mu_r} \text{grad}_{2D} u_z, \text{grad}_{2D} w_z \right)_{0,\Omega} + \\ & + \left( \frac{1}{\mu_r} \text{curl}_{2D} \mathbf{u}_t, \text{curl}_{2D} \mathbf{w}_t \right)_{0,\Omega} + \\ & + j \frac{\omega}{c_0} \left( \frac{\zeta_2}{\mu_r} \mathbf{u}_t, \text{grad}_{2D} w_z \right)_{0,\Omega} + \\ & - j \frac{\omega}{c_0} \left( \frac{\zeta_2}{\mu_r} \text{grad}_{2D} u_z, \mathbf{w}_t \right)_{0,\Omega} + \\ & - \frac{\omega^2}{c_0^2} (\varepsilon_r u_z, w_z)_{0,\Omega} + \\ & - \frac{\omega^2}{c_0^2} \left( \frac{1 + \varepsilon_r \mu_r - \zeta_1}{\mu_r} \mathbf{u}_t, \mathbf{w}_t \right)_{0,\Omega} + \\ & + j\omega \mu_0 (Y(\gamma_0 u_z), \gamma_0 w_z)_{0,\Gamma} + \\ & + j\omega \mu_0 (Y(\mathbf{u}_t \cdot \mathbf{l}), \mathbf{w}_t \cdot \mathbf{l})_{0,\Gamma}, \end{aligned} \quad (17)$$

for all  $\mathbf{u}, \mathbf{w} \in U$  and  $l$  is the following antilinear form:

$$\begin{aligned} l(\mathbf{w}) = & -j\omega \mu_0 (J_{ez}, w_z)_{0,\Omega} + \\ & - \left( \frac{\zeta_1}{\mu_r} \hat{\mathbf{z}} \times \mathbf{J}_{mt}, \text{grad}_{2D} w_z \right)_{0,\Omega} + \\ & - j\omega \mu_0 (f_{Rz}, \gamma_0 w_z)_{0,\Gamma} + \\ & - \left( \frac{1}{\mu_r} J_{mz}, \text{curl}_{2D} \mathbf{w}_t \right)_{0,\Omega} + \\ & - j\omega \mu_0 (\mathbf{J}_{et}, \mathbf{w}_t)_{0,\Omega} + \\ & + j \frac{\omega}{c_0} \left( \frac{\zeta_2}{\mu_r} \hat{\mathbf{z}} \times \mathbf{J}_{mt}, \mathbf{w}_t \right)_{0,\Omega} + \\ & - j\omega \mu_0 (f_{Rl}, \mathbf{w}_t \cdot \mathbf{l})_{0,\Gamma}, \end{aligned} \quad (18)$$

for all  $\mathbf{w} \in U$ .

The reader can notice that, whenever  $\beta = 0$  everywhere in  $\Omega$  (which implies  $\zeta_2 = 0$  in  $\Omega$ ), the problem splits into two disjoint problems, one for the axial component  $E_z$ , the other for the transverse part

$\mathbf{E}_t$ . These two disjoint problems are the traditional, two-dimensional variational problems, formulated in terms of  $E_z$  or  $\mathbf{E}_t$ , in the presence of motionless isotropic media.

In [12] we showed that under some non-restrictive hypotheses any electromagnetic problem of the class considered is well posed. In particular, for any problem of interest we can find a unique solution  $(\mathbf{E}, \mathbf{B}, \mathbf{H}, \mathbf{D})$  belonging to  $U \times (L^2(\Omega))^3 \times U \times (L^2(\Omega))^3$  and depending continuously on  $\mathbf{J}_e, \mathbf{J}_m \in (L^2(\Omega))^3$  and on  $f_{Rz}, f_{Rl} \in L^2(\Gamma)$ . It is worth mentioning that, due to the bianisotropic behaviour of the media in motion, all unknown fields will have, in general, all three components, even if the scatterers are illuminated by simple fields.

### III. FINITE ELEMENT APPROXIMATION

Under some additional assumptions, in [12] we also found that a finite element method, based on the above variational formulation and exploiting a first-order Lagrangian approximation for the axial component and a first-order edge element approximation for the transverse part, determines  $(\mathbf{E}_h, \mathbf{B}_h, \mathbf{H}_h, \mathbf{D}_h) \in U_h \times (L^2(\Omega))^3 \times (L^2(\Omega))^3 \times (L^2(\Omega))^3$  which converges, as  $h$  goes to zero, to  $(\mathbf{E}, \mathbf{B}, \mathbf{H}, \mathbf{D})$  in  $U \times (L^2(\Omega))^3 \times (L^2(\Omega))^3 \times (L^2(\Omega))^3$ . In the previous statement  $U_h$  is the finite dimensional subspace of  $U$  generated by the indicated elements (first-order Lagrangian and first-order edge elements) for a specific triangulation of  $\Omega$  and  $h$  denotes, as usual, the maximum diameter of all elements of the triangulation [14] (p. 131).

In [12] no specific considerations related to the implementation of finite element codes were provided. These considerations could be useful for our next developments and, for this reason, we present here the main points. Suppose that for any mesh adopted, fixing a given  $U_h$ , we order the degrees of freedom by placing those related to  $E_{hz}, [e_z] \in \mathbb{C}^{nn}$ , in the first part of the vector  $[e] \in \mathbb{C}^{nn+ne}$  of the unknowns while those related to  $\mathbf{E}_{ht}, [e_t] \in \mathbb{C}^{ne}$ , are in its second and last part. In the previous formulas,  $nn$  (respectively,  $ne$ ) refers to the number of nodes (respectively, edges) of the mesh considered. With this convention, by firstly considering the  $nn$  test functions like  $\mathbf{w}_h = (0, 0, w_{hz})$  and, then, the  $ne$  test functions like  $\mathbf{w}_h = \mathbf{w}_{ht}$ , one can easily deduce that the general form of the final matrix equation obtained from (16), (17) and (18), with  $\mathbf{E}, \mathbf{u}, \mathbf{w}$  and  $U$  replaced, respectively, by  $\mathbf{E}_h, \mathbf{u}_h, \mathbf{w}_h$  and  $U_h$ , is:

$$[A][e] = [l], \quad (19)$$

where the entries of  $[l] \in \mathbb{C}^{nn+ne}$  are given by  $l(\mathbf{w}_h)$ , for all test functions considered. The order for its entries is given by the order considered for the test functions and, in analogy to the decomposition of  $[e]$  in terms of  $[e_z]$  and  $[e_t]$ , we get  $[l_z] \in \mathbb{C}^{nn}$ , in the first part of  $[l]$

and  $[l_t] \in \mathbb{C}^{ne}$  in the second and last one.  $[A]$  is given by:

$$[A] = \begin{bmatrix} [A_{zz}] & [A_{zt}] \\ [A_{tz}] & [A_{tt}] \end{bmatrix}. \quad (20)$$

In this formula,  $[A_{zz}]$ ,  $[A_{zt}]$ ,  $[A_{tz}]$  and  $[A_{tt}]$  are complex matrices whose entries are deduced directly from (17):

$$[A_{zz}]_{ij} = \left( \frac{\zeta_1}{\mu_r} \text{grad}_{2D} w_{hzj}, \text{grad}_{2D} w_{hzi} \right)_{0,\Omega} + \frac{\omega^2}{c_0^2} (\varepsilon_r w_{hzj}, w_{hzi})_{0,\Omega} + j\omega\mu_0 (Y(\gamma_0 w_{hzj}), \gamma_0 w_{hzi})_{0,\Gamma}, \quad i, j \in 1, \dots, nn, \quad (21)$$

$$[A_{zt}]_{ij} = j \frac{\omega}{c_0} \left( \frac{\zeta_2}{\mu_r} \mathbf{w}_{htj}, \text{grad}_{2D} w_{hzi} \right)_{0,\Omega}, \quad i \in 1, \dots, nn, \quad j \in 1, \dots, ne, \quad (22)$$

$$[A_{tz}]_{ij} = -j \frac{\omega}{c_0} \left( \frac{\zeta_2}{\mu_r} \text{grad}_{2D} w_{hzj}, \mathbf{w}_{hti} \right)_{0,\Omega}, \quad i \in 1, \dots, ne, \quad j \in 1, \dots, nn, \quad (23)$$

$$[A_{tt}]_{ij} = \left( \frac{1}{\mu_r} \text{curl}_{2D} \mathbf{w}_{htj}, \text{curl}_{2D} \mathbf{w}_{hti} \right)_{0,\Omega} + \frac{\omega^2}{c_0^2} \left( \frac{1 + \varepsilon_r \mu_r - \zeta_1}{\mu_r} \mathbf{w}_{htj}, \mathbf{w}_{hti} \right)_{0,\Omega} + j\omega\mu_0 (Y(\mathbf{w}_{htj} \cdot \mathbf{l}), \mathbf{w}_{hti} \cdot \mathbf{l})_{0,\Gamma}, \quad i, j \in 1, \dots, ne. \quad (24)$$

In this case, too, whenever  $\beta = 0$  everywhere in  $\Omega$ , the two matrices  $[A_{zt}]$  and  $[A_{tz}]$  become trivial and the discrete problem splits into two disjoint parts: one for  $[e_z]$ , the other for  $[e_t]$ . These are the classical two-dimensional problems for TM and TE polarized fields, respectively, in the presence of motionless media.

It is important to note that the second and third addends in the right-hand side of (21) are independent of  $\beta$ . The same is true for the first and third addends in the right-hand side of (24). Taking account of (6) one easily deduces that, for small values of the maximum of  $|\beta|$ ,  $\zeta_2 \approx \beta(\mu_r \varepsilon_r - 1)$  and all entries of  $[A_{zt}]$  and  $[A_{tz}]$  have magnitudes which are smaller or equal to numbers proportional to the maximum of  $|\beta|$ , under the same conditions. Finally, the addends of the right-hand sides of (21) and (24) which depend on  $\beta$ , again for small values of the maximum of  $|\beta|$ , involve  $\zeta_1 \approx 1 + (1 - \mu_r \varepsilon_r) \beta^2$  and  $1 + \varepsilon_r \mu_r - \zeta_1 \approx \varepsilon_r \mu_r - (1 - \mu_r \varepsilon_r) \beta^2$ . Thus, the considered quantities are only slightly affected by the motion, if the maximum of  $|\beta|$  is small.

In order to solve the algebraic linear system (19) several algorithms can be adopted. Among these, we consider iterative solvers, which are very popular for the solution of linear systems arising in finite element simulations [19] (pp. 382, 383, 396-405), [20] (p. 334). The stopping criteria we adopt in all cases, which defines when the iterative solution has reached convergence, is "criterion 2" of [21] (p. 60). For the reader convenience

we recall that this criterion requires at the beginning the calculation of the Euclidean norm  $||[L]||$  of  $[L]$ . At iteration  $i$  the approximate solution  $[e]_i$  determines an error  $||[A][e]_i - [L]||$ . The iterative process is stopped when the condition  $||[A][e]_i - [L]|| < \delta ||[L]||$  is satisfied, where  $\delta$  is the so-called residual. Usually,  $\delta$  is a small value in the range  $[10^{-12}, 10^{-9}]$  when double precision arithmetic is used [21] (pp. 58-60).

If we assume TM polarized plane wave as the incident wave, then as the maximum value of  $|\beta|$  goes to zero, the Euclidean norm of components of  $[e_t]$  goes to zero whereas that of components of  $[e_z]$  goes to the non-zero value of the corresponding motionless problem. Hence the loss of number of significant digits due to round-off errors becomes large for the transverse components. Since for low values of  $|\beta|$ ,  $||[e_t]||$  becomes proportional to  $|\beta|$  and  $||[e_z]||$  remains almost constant, the ratio  $\frac{||[e_t]||}{||[e_z]||}$  becomes proportional to  $|\beta|$  as well. We know that  $\frac{||\Delta[e]||}{||[e]||} \leq K_A \Delta_{roundoff}$ . Here  $\Delta[e]$  is the error in the solution due to round-off,  $K_A$  the condition number of matrix  $[A]$ .  $\Delta_{roundoff} = (\frac{||\Delta[A]||}{||[A]||} + \frac{||\Delta[L]||}{||[L]||} + \delta)$ , where  $\Delta[A]$  and  $\Delta[L]$  denote change in  $[A]$  and  $[L]$  due to round-off. Now assuming that the round-off errors are uniformly distributed across the elements of  $[e]$ , it is easy to deduce that  $\frac{||\Delta[e_t]||}{||[e_t]||} \leq \frac{nn+ne}{ne} \frac{||[e]||}{||[e_t]||} K_A \Delta_{roundoff}$ . At low values of  $|\beta|$  we can consider  $||[e]|| \approx ||[e_z]||$  and that  $\Delta_{roundoff} \approx \delta$ . Thus we can write:

$$\frac{||\Delta[e_t]||}{||[e_t]||} \leq \frac{nn+ne}{ne} \frac{||[e_z]||}{||[e_t]||} K_A \delta. \quad (25)$$

Thus, it can be seen that the residual error on the transverse component can be magnified by a factor of  $\frac{nn+ne}{ne} \frac{||[e_z]||}{||[e_t]||} K_A$  for small  $|\beta|$  values. If the maximum allowable error is  $\delta_{max}$ , then it needs to be ensured that  $\frac{nn+ne}{ne} \frac{||[e_z]||}{||[e_t]||} \leq \frac{\delta_{max}}{K_A \delta}$ .

#### IV. DEFINITION OF A TEST CASE AND OF THE RELEVANT ERRORS

In order to deduce some results on the accuracy of finite element solutions in the presence of axially moving cylinders we need to consider simple problems which allow the calculation of the fields of interest with other reliable tools. For this reason, we consider single canonical cylinders moving in the axial direction. Analogous studies have been performed under the same type of simplifying assumptions related to the inhomogeneity of the media involved, the particular shapes of the scatterers or the illuminating field (see, for example, [20] (p. 188) or [22]). For this reason, we consider the case of a circular cylinder hosted in vacuum and illuminated by a uniform plane wave. In particular, the cylinder axis is assumed to be the  $z$  axis and the

cylinder cross-section will have a radius  $R \leq 0.2$  m. The medium inside the cylinder is assumed to be homogeneous and, in its rest frame, isotropic and not dispersive. It will be characterized by  $\mu_r = 1$ . We assume that such a medium is in uniform motion along the  $z$  axis. Finally, we will consider a TM-polarized incident plane wave impinging orthogonally on the cylinder and defined by  $E_z^{inc} = E_0 e^{j2\pi f \sqrt{\mu_0 \epsilon_0} y}$ ,  $f$  being the frequency always equal to 1 GHz except for one case when  $f = 500$  MHz will be considered. The choice of the simple canonical problem just described was motivated not only by the possibility of finding semi-analytical solutions by using other tools, but also by the possible application of this study to the reconstruction of  $\beta$  profiles, as it will be explained later on. In the following we will consider several different values for the normalized axial speed  $\beta$  of the cylinder, for its relative permittivity  $\epsilon_r$  (in its rest frame) and for its radius  $R$ .

For problems of this class an efficient semi-analytical procedure, able to compute very good approximations of their solutions was proposed by Yeh [4] (see also Remark 5 of [15]).

The scattering problems just defined are numerically studied by using a finite element simulator based on the considerations reported in the previous section. The domain of numerical investigation we have adopted is, in any case, a polygon approximating a circle in the  $(x, y)$  plane, whose center is at the origin and whose radius is equal to 0.4 m. Such a numerical domain is discretized by using several meshes. In particular, all these meshes are obtained by using  $n$  concentric circles and, starting from the center, the innermost circle is divided into 6 segments, the next one in 12 and so on. The domain is thus divided almost uniformly into  $6n^2$  triangles, with  $1 + 3n + 3n^2$  nodes,  $3n + 9n^2$  edges and  $6n$  boundary edges. An example of one mesh of this type can be found in Fig. 1 of [22] (the reader has to consider just the upper base of the three-dimensional cylinder shown in that figure). In the following  $n$  will be equal to 20, 40, 80, 120, 160 or 200. Correspondingly, we will get a mesh characterized, respectively, by  $h$  equal to 0.0285874, 0.0143858, 0.00721629, 0.00481608, 0.00361402 or 0.00289216 m, with, respectively, 1261, 4921, 19441, 43561, 77281, 120601 nodes, 2400, 9600, 38400, 86400, 153600, 240000 elements, 3660, 14520, 57840, 129960, 230880, 360600 edges, and 120, 240, 480, 720, 960, 1200 boundary edges. All the indicated values of  $n$  can be used to discretize scatterers whose radius  $R$  is a multiple of 2 cm (respectively, 1 cm if we avoid using  $n = 20$ ).

It is very important to point out that, in order to keep the analysis as simple as possible, we avoided considering meshes made up of curved triangles. This means, in particular, that, since the scatterer cross-

section is not a polygon, in all our simulations we suffer from a kind of non-conformity [14] (p. 209). As a matter of fact, the scatterer has not the shape of the numerical scatterer and, moreover, the domain of numerical investigation and the numerical scatterer itself change their shapes for different values of  $n$ . By the same token, we adopted the semi-analytical procedure defined by Yeh [4] (the series are truncated after the first 60 terms for these calculations) to compute the piecewise constant data  $f_{Rzh}$  and  $f_{Rlh}$  enforcing the inhomogeneous terms in the admittance boundary conditions considered on  $\Gamma$  for the discretized problem (the admittance  $Y$  is set to  $Y_0 = \sqrt{\frac{\epsilon_0}{\mu_0}}$  in any case). In this way, we get another violation of conformity, according to [14] (p. 183). The reader should note that these violations of conformity were not considered in [12] and formally the convergence results we deduced there could not be applied. In the following, however, according to a well-established approach, we neglect this technical problem and assume that our convergence results do apply to the cases considered. The numerical results we will show provide a heuristic proof of this statement.

An evaluation of the numerical errors of the finite element solutions could now be performed. However, we introduce an additional simplification which allows us to find good estimates of the errors by exploiting finite element calculations. In particular, we will call  $E_{z,h,analytic}$  and  $H_{z,h,analytic}$  the first-order Lagrangian element expansions which are deduced by evaluating their degrees of freedom with the semi-analytical procedure proposed by Yeh [4]. Analogously,  $\mathbf{E}_{t,h,analytic}$  will refer to the first-order edge element expansion which is deduced by evaluating its degrees of freedom with Yeh's procedure. In the above three calculations the series involved in Yeh's procedure are truncated after the first 40 terms. The reader should observe that  $H_{z,h,analytic}$  is not related to  $\mathbf{E}_{t,h,analytic}$  by the usual Maxwell's curl equation (while  $H_{hz}$  is, by definition, equal to  $-\frac{1}{j\omega\mu_0\mu_r}\text{curl}_{2D}\mathbf{E}_{ht}$ ; see equation (3.3) and the considerations below Theorem 5.3 at the end of Section 5 of [12]). As a matter of fact, it is very well known that the curl of a first-order edge element field is piecewise constant while  $H_{z,h,analytic}$  is, as it has already been pointed out, a first-order Lagrangian element field. The decision to consider  $H_{z,h,analytic}$  and  $\mathbf{E}_{t,h,analytic}$  not related by the usual Maxwell's curl equation was made for the possible application of our results to inverse problem techniques aiming at the reconstruction of  $\beta$  profile, as it will be further clarified later on.

The previous definitions allow us to introduce a set of (estimates of) absolute errors on  $E_z$ ,  $\mathbf{E}_t$  and  $H_z$  by

using different relevant norms or semi-norms. Thus we have:

$$e_{z,a,l2} = \|E_{z,h,analytic} - E_{hz}\|_{0,\Omega}, \quad (26)$$

$$e_{z,a,h1} = \|E_{z,h,analytic} - E_{hz}\|_{1,\Omega}, \quad (27)$$

$$e_{z,a,semi} = \|\text{grad}_{2D}E_{z,h,analytic} - \text{grad}_{2D}E_{hz}\|_{0,\Omega}, \quad (28)$$

$$e_{t,a,l2} = \|\mathbf{E}_{t,h,analytic} - \mathbf{E}_{ht}\|_{0,\Omega}, \quad (29)$$

$$e_{t,a,\Gamma} = \|(\mathbf{E}_{t,h,analytic} - \mathbf{E}_{ht}) \cdot \mathbf{I}\|_{0,\Gamma}, \quad (30)$$

$$e_{a,hz} = \|H_{z,h,analytic} - H_{hz}\|_{0,\Omega}. \quad (31)$$

In the presence of a constant relative permeability  $e_{a,hz}$  can be considered as an estimate of  $\frac{1}{\omega\mu_0\mu_r}e_{t,a,semi}$ , where,

$$e_{t,a,semi} = \|\text{curl}_{2D}\mathbf{E}_{t,h,analytic} - \text{curl}_{2D}\mathbf{E}_{ht}\|_{0,\Omega}, \quad (32)$$

so that we can also consider:

$$e_{t,a,u2D} = \sqrt{e_{t,a,l2}^2 + e_{t,a,\Gamma}^2 + e_{t,a,semi}^2}, \quad (33)$$

as an estimate of the  $U_{2D}$  norm error.

Relative errors are important, too, especially for the problems of interest, due to the huge variation of some of the quantities involved. For this reason, we consider the following relative errors:  $e_{z,r,l2}$ ,  $e_{z,r,h1}$ ,  $e_{z,r,semi}$ ,  $e_{t,r,l2}$ ,  $e_{t,r,\Gamma}$  and  $e_{r,hz}$ , which are defined by dividing the corresponding absolute error by the norm of the "analytic" part involved in the definition of the absolute error itself. Once more, under the indicated condition,  $e_{r,hz}$  can be considered as an estimate of  $e_{t,r,semi}$ .

For the TM-polarized incident field considered, it is important to emphasize that, for a motionless cylinder, the solution presents  $\mathbf{E}_t = 0$ . Moreover, for small values of  $|\beta|$  it is known that  $\|\mathbf{E}_t\|_{U2D}$  is small [16]. Thus, all relative errors related to the transverse part of the electric field (that is,  $e_{t,r,l2}$ ,  $e_{t,r,\Gamma}$ ,  $e_{r,hz}$ ,  $e_{t,r,semi}$ ) are expected to become larger and larger as  $|\beta|$  goes to zero. At the same time, it could be important to analyze the behaviours of these errors, especially under the indicated conditions, because, on the one hand, good electromagnetic imaging techniques, able to recover the profile of the axial speed, exploits only, for the indicated incident polarization, data related to  $H_z = \frac{j}{\omega\mu_0}\text{curl}_{2D}\mathbf{E}_t$  [16]. On the other hand, the finite element method we are studying can be exploited to provide approximate values of  $H_z$  at the measurement points for any trial solution for the  $\beta$  profile considered by the inverse procedure itself [16].

For this reason, in the next section, a part of our numerical analysis will be devoted to considerations related to the reliability of finite element solutions in terms of  $H_z$  and, in particular, of  $e_{a,hz}$  and  $e_{r,hz}$ . This part of the analysis was, actually, the initial motivation for this study.

*Remark 1:* In many applications the reconstruction of the profiles of  $\epsilon_r$  and  $\beta$  are of interest [8]. For the indicated polarization of the incident field, the axial

component of the electric field is the most important quantity for the reconstruction of  $\varepsilon_r$  while the axial component of the magnetic field is crucial for the reconstruction of  $\beta$  [16]. In particular, under some non-restrictive hypotheses, the reconstruction of  $\varepsilon_r$  can be carried out neglecting any movement and by using data related to  $E_z$  only. The estimated  $\varepsilon_r$  is then adopted as an input data for the reconstruction of the axial speed profile. For the indicated reasons, a finite element code based on a formulation expressed in terms of  $\mathbf{E}$  was considered. In our previous considerations we focused in particular on the generation of reliable data for the second step of the reconstruction process, devoted to the estimate of the  $\beta$  profile, simply because the reconstruction algorithms adopted for determining  $\varepsilon_r$  have been studied for decades [23] while those adopted to recover  $\beta$  are not so standard in the framework of microwave imaging techniques.

*Remark 2:*  $e_{r,hz}$  could also be referred to a proper subdomain  $\Omega_m$  of  $\Omega$ . We could use  $e_{r,hz,\Omega_m}$  as an alternative symbol in this case. The subdomain can also be of zero measure (e.g., made up of curves or points) because the involved quantities ( $H_{z,h,analytic}$  and  $H_{hz}$ ) are continuous in  $\Omega$ . However, in this case we have to change the norm in the definition of the error (the  $L^2(\Omega)$  norm is not meaningful anymore).

The results provided in [12] can be applied to the problems here considered if some conditions involving  $\varepsilon_r$  and  $\beta$  are satisfied (see, in particular, Section 7 of [12]). In particular, in order to show some examples, we can say that in the presence of a cylinder having  $\varepsilon_r = 2$  the problem is well-posed and the convergence of finite element approximations is guaranteed (neglecting the conformity violations already pointed out) whenever  $|\beta| \leq 0.264308$ . For other cylinder media, for example when  $\varepsilon_r = 1.1$  or  $\varepsilon_r = 8$ , the upper bounds for  $|\beta|$  are 0.777053 or 0.0826784, respectively. The reader should notice that the corresponding upper bounds for the axial speed values are really impressive (equal to  $\approx 232954629$  m/s when  $\varepsilon_r = 1.1$ ,  $\approx 79237545$  m/s when  $\varepsilon_r = 2.0$  and  $\approx 24786361$  m/s when  $\varepsilon_r = 8.0$ ) and that they are not much smaller than the values of the normalized speed of light in the media considered (given by  $\frac{1}{\sqrt{1.1}} \approx 0.953463$ ,  $\frac{1}{\sqrt{2}} \approx 0.707107$  and  $\frac{1}{\sqrt{8}} \approx 0.353355$ , respectively).

## V. NUMERICAL RESULTS

As was already pointed out, for the defined test case we consider several values of  $\varepsilon_r$ ,  $\beta$ ,  $R$  and  $n$ . The effects of these parameters on the errors related to  $E_z$ ,  $\mathbf{E}_t$  and  $H_z$  are studied. In particular, the results related to  $E_z$  are shown in the first subsection while in the second one we provide considerations on the errors on  $\mathbf{E}_t$  and  $H_z$ . From these two sub-sections we establish accuracy of the numerical simulations and the convergence behaviour of

the components. In the third subsection, we consider the problematic cases where accuracy of the results related to  $\mathbf{E}_t$  and  $H_z$  start dropping. This is due to the finite precision of the calculations which start to accumulate round-off errors when the bi-anisotropic effect is too weak to give a significant cross-polarized component.

### A. Numerical results related to $E_z$

The first results on  $E_z$  we show are all related to cases involving cylinders characterized by  $\varepsilon_r = 2$  and  $R = 0.2$  m. In particular, in Fig. 1 we report the absolute errors related to the axial component of the electric field,  $e_{z,a,h1}$ ,  $e_{z,a,l2}$  and  $e_{z,a,semi}$ , versus  $h$  for two values of  $\beta$ :  $\beta = 0$  and  $\beta = 0.25$ . As the reader can easily check, it is not possible to distinguish the results of the  $\beta = 0$  case from those obtained when  $\beta = 0.25$ . Many other simulations have been performed, for  $\beta = 5 \cdot 10^{-m}$ ,  $m = 1, \dots, 15$ . These additional results are not reported in Fig. 1 because the plots would be the same as those already shown. In the figure two plots proportional to  $h$  and  $h^2$  are provided, too, in order to be able to determine the rate of convergence of the results as functions of  $h$ .

As it was pointed out in Section III the results for the  $\beta = 0$  case can be obtained by using a traditional two-dimensional finite element algorithm based on first-order Lagrangian elements (dealing with isotropic media at rest). There is nothing new in the results shown for this case, as it is very well-known [19]; we can simply observe that the absolute errors related to  $E_z$  behave like  $h^2$  and that  $e_{z,a,semi}$  is much larger than  $e_{z,a,l2}$  so determining almost completely  $e_{z,a,h1}$ .

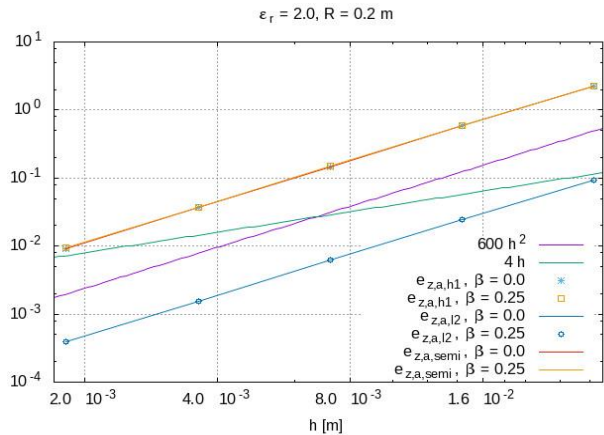


Fig. 1. Behaviour of  $e_{z,a,h1}$ ,  $e_{z,a,l2}$  and  $e_{z,a,semi}$  versus  $h$ , when the cylinder is at rest or moves with  $\beta = 0.25$ . The cylinder is assumed to have  $R = 0.2$  m and to be made up of a material having  $\varepsilon_r = 2$  at rest. Two plots proportional to  $h$  and  $h^2$  are provided, too.

The results corresponding to  $\beta = 0.25$  (determining a huge axial speed of 74948114.5 m/s) show that the finite element capability of approximating the axial

component of the true solution is the same as in the case all media are at rest. In particular, the convergence rate remains quadratic and, taking account of all simulations performed, we can say that this property is completely independent of  $\beta$ . For the same reason, no figure related to the relative errors on  $E_z$  is provided.

It could be interesting to observe that  $\beta = 0.25$  is close to the upper bound for  $\beta$  reported in Section IV and has a significant effect on  $E_z$ . These effects are not shown in a figure for space reasons. We simply observe that, for example,  $Re(E_{hz}) = -0.0549$  V/m at the origin in the  $\beta = 0$  case while  $Re(E_{hz}) = -0.132$  V/m at the same point when  $\beta = 0.25$ . Both values are obtained by using a mesh with  $n = 320$ .

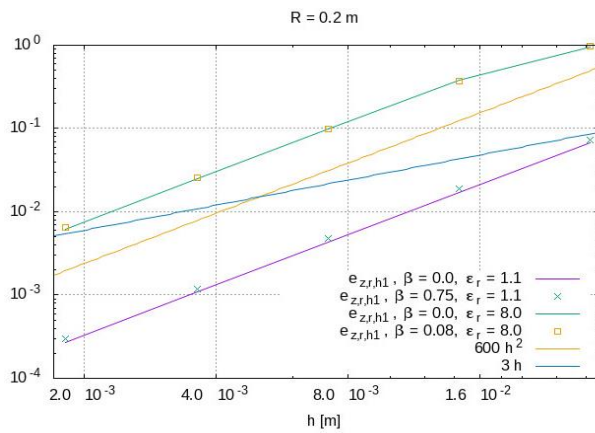


Fig. 2. Behaviour of  $e_{z,r,h1}$  versus  $h$  for different values of  $\beta$  and  $\epsilon_r$ . In particular, for any value of  $\epsilon_r$  one of the largest possible normalized axial speed values is considered in addition, for both cases, to  $\beta = 0$ . The scatterer radius is  $R = 0.2$  m.

The previous considerations on the independence of the accuracy of the  $E_z$  results from the value of  $\beta$  seem to be correct even when the other parameters are changed. For example, if we consider  $\epsilon_r = 1.1$  or  $\epsilon_r = 8$  we get the relative errors shown in Fig. 2. The reader can easily observe that the error behaviour in both cases does not depend on  $\beta$  and that the convergence rate remains  $O(h^2)$ . However, for any given mesh, the relative errors on  $E_z$  are larger for  $\epsilon_r = 8$  than for  $\epsilon_r = 1.1$ , due to the reduction of the wavelength in the scatterer by a factor approximately equal to  $2\sqrt{2}$ . This effect is very well known and does not require any additional comment [19], [20] (p. 344).

Changes on  $R$  are considered, too, but the conclusion for the errors on  $E_z$  remains unaltered. When  $\epsilon_r = 2$  and  $R = 0.02$  m we get, by using a mesh with  $n = 320$ ,  $e_{z,r,h1} = 0.269 \cdot 10^{-3}$  if  $\beta = 0$  and  $e_{z,r,h1} = 0.270 \cdot 10^{-3}$  if  $\beta = 0.25$ . The corresponding quantities obtained when  $\epsilon_r = 2$  and  $R = 0.2$  m (with the same mesh) are

$e_{z,r,h1} = 0.557 \cdot 10^{-3}$  if  $\beta = 0$  and  $e_{z,r,h1} = 0.563 \cdot 10^{-3}$  if  $\beta = 0.25$ .

Overall we can say that the finite element approximation of  $E_z$ , in the presence of axially moving cylinders illuminated by TM-polarized incident plane waves, is as satisfactory as in the presence of motionless scatterers, independently of all values of the parameters considered.

## B. Numerical results related to $E_t$ and $H_z$

In this sub-section we examine the errors related to the cross-polarized component  $E_t$  and the related magnetic field component  $H_z$ . These quantities are zero in the motionless case, and arises because of the bi-anisotropic effect due to motion. The convergence of these components are examined and the accuracy of the simulation is established for a large range of parameters like  $\beta$ ,  $\epsilon_r$  and  $R$  of the scatterer.

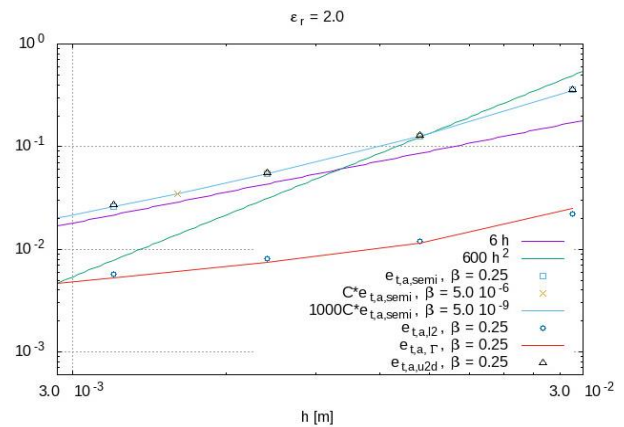


Fig. 3. Behaviour of  $e_{t,a,u2d}$ ,  $e_{t,a,l2}$ ,  $e_{t,a,\Gamma}$  and  $e_{t,a,semi}$  versus  $h$ , when the cylinder moves with  $\beta = 0.25$ . Plots proportional to  $e_{t,a,semi}$  is also reported for  $\beta = 5 \cdot 10^{-m}$ ,  $m = 6, 9$ .  $C = 5 \cdot 10^7$ . The cylinder is assumed to have  $R = 0.2$  m and to be made up of a material having  $\epsilon_r = 2$  at rest. Two plots proportional to  $h$  and  $h^2$  are provided, too.

In Fig. 3 some results related to the absolute errors on  $E_t$  are shown. The case  $\beta = 0$  is not meaningful for the present analysis because, for the test case considered, the solution has  $E_t = 0$  in  $\Omega$  and the finite element method is able to compute  $E_{ht} = 0$  in  $\Omega$  for any mesh considered. For this reason, the results refer to cases in which  $\beta \neq 0$ . A complete set of results is shown for  $\beta = 0.25$ . One can observe that  $e_{t,a,semi}$  is much larger than  $e_{t,a,l2}$  and  $e_{t,a,\Gamma}$  so that  $e_{t,a,u2d} \approx e_{t,a,semi}$ . Moreover, it can be observed that the convergence rate is  $O(h)$  for all errors considered. The values of  $e_{t,a,semi}$  for  $m = 6$  and  $m = 9$  are also shown in the figure. Over this large range of  $\beta$ , the convergence behaviour is not affected.

Now we verify what happens when the cylinder is made up of other materials. As in the previous subsection, we will consider  $\varepsilon_r = 1.1$  and  $\varepsilon_r = 8$  along with  $\varepsilon_r = 2$ . Figure 4 shows the relative error in  $H_z$  for these cases. The results are analogous to Fig. 2 except for the slower rate of convergence. Again, an increase in  $\varepsilon_r$  results in an increase in discretization error, due to the reduction in wavelength. The errors remain largely independent of  $\beta$  over a wide range, with  $\beta$  which could be as low as  $5 \cdot 10^{-9}$ .

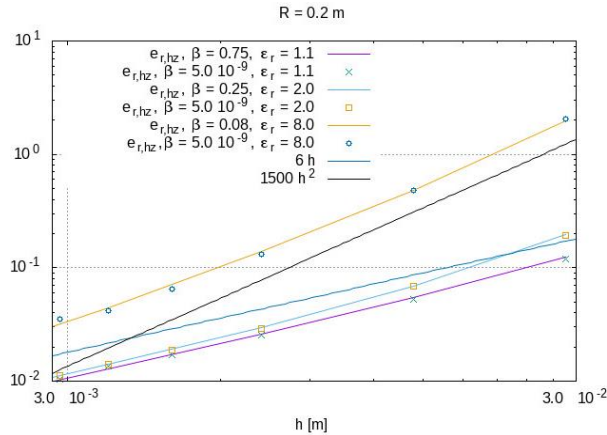


Fig. 4. Behaviour of  $e_{r,hz}$  versus  $h$  for different values of  $\beta$  and  $\varepsilon_r$ . In particular,  $\varepsilon_r = 1.1$ ,  $\varepsilon_r = 2$  and  $\varepsilon_r = 8$  are considered. In each case a value close to the upper bound of  $\beta$  is taken along with  $\beta = 5 \cdot 10^{-9}$ . Two plots proportional to  $h$  and  $h^2$  are provided, too.

Finally, we study the effect of changing the radius of the scatterer. Along with the  $R = 0.2$  m considered for the previous instances,  $R = 0.1$  m and  $R = 0.05$  m were examined. It is not appropriate to consider too small values of  $R$ . This is because of the non-conformity due to polygonal approximation of the circular boundary of the scatterer, as was explained in section IV. Instead the frequency is reduced so that the ratio of  $R$  to the wavelength reduces, which is expected to give an equivalent effect on discretization error. Hence, we study  $f = 500$  MHz in addition to  $f = 1$  GHz considered in the preceding cases. The discretization error is not affected much by the reduction in radius of the scatterer. With  $n = 120$  and  $f = 1$  GHz, for  $\beta \leq 5 \cdot 10^{-10}$  the relative errors remain below 4% for all variations of  $R$  considered. As for the effect of reducing  $f$ , the discretization error drops below 2% which is expected from the increase in wavelength.

The results in this subsection and the last one show as expected [12], that the finite element approximation is converging to the true solution (notwithstanding the two violations of conformity pointed out in Section IV). However, the results related to  $\mathbf{E}_t$  and  $H_z$  do start

becoming worse due to round-off errors when the magnitude of these quantities become small. We consider such cases in the next section.

### C. Problematic results related to $\mathbf{E}_t$ and $H_z$

In this subsection, we consider the cases when the round-off error becomes significant. As indicated by Equation (25), when the cross-polarized component becomes too low, the round-off error becomes more and more significant. Although we get good accuracy for the co-polarized component, the cross-polarized component could be unreliable. This could be the case with very low values of  $\beta$ ,  $\varepsilon_r$  or  $R$ . Hence, in these critical cases, one needs to be careful with the simulations.

In Fig. 5 the relative errors pertaining to  $H_z$  are shown with respect to  $h$  for small  $\beta$  values with  $m = 10, \dots, 15$ . For sufficiently small values of  $h$ , although the errors remain less than 10% up to  $m = 12$ , they start increasing for finer discretizations. The results become completely unreliable for smaller values of  $\beta$ . A finer discretization need not produce a decrease in the error in these critical cases, since the increase of round-off error is dominating over the reduction in discretization error. These results suggest that one should be careful in dealing with these delicate cases. One may have to make use of higher precision calculations to accurately solve these problems.

In Fig. 6 we examine the effect of different permittivity values along with small  $\beta$ . Again  $\varepsilon_r = 1.1$  and  $\varepsilon_r = 8.0$  are taken and we consider  $m = 10, 11, 12$ . The trend remains similar to that for  $\varepsilon_r = 2.0$  in Fig. 5. For  $\varepsilon_r = 8.0$ , the errors start off large, due to higher discretization error, and goes on becoming worse due to round-off. For  $\varepsilon_r = 1.1$ , the discretization error is smaller than that for  $\varepsilon_r = 2.0$ . But once the round-off error becomes significant it can increase very quickly.

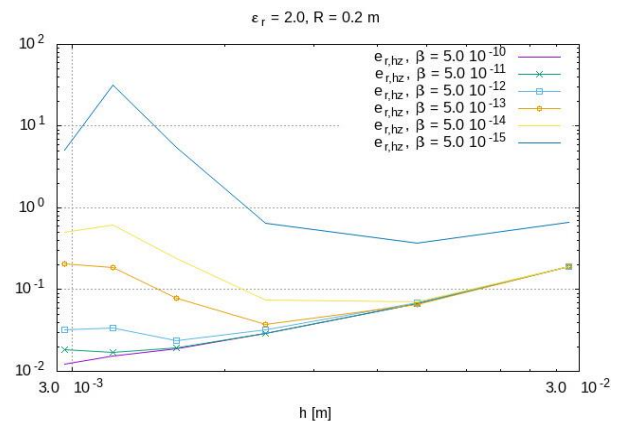


Fig. 5. Behaviour of  $e_{r,hz}$  versus  $h$ , when the cylinder moves with  $\beta = 5 \cdot 10^{-m}$ ,  $m = 10, \dots, 15$ . The cylinder is assumed to have  $R = 0.2$  m and to be made up of a material having  $\varepsilon_r = 2$  at rest.

In Fig. 7 the relative error on  $H_z$  is plotted against  $\beta$  values. Three different values are considered for the radius of scatterer,  $R = 0.2, R = 0.1$  and  $R = 0.05$  meters. The calculations are done for two frequency values  $f = 1$  GHz and  $f = 500$  MHz. The bi-anisotropic effect reduces as the scatterer becomes smaller, which might result in a higher round-off error. This could explain why the error starts increasing at  $m = 11$  in the case of  $f = 1$  GHz whereas for all other cases the error is stable till  $m = 12$ .

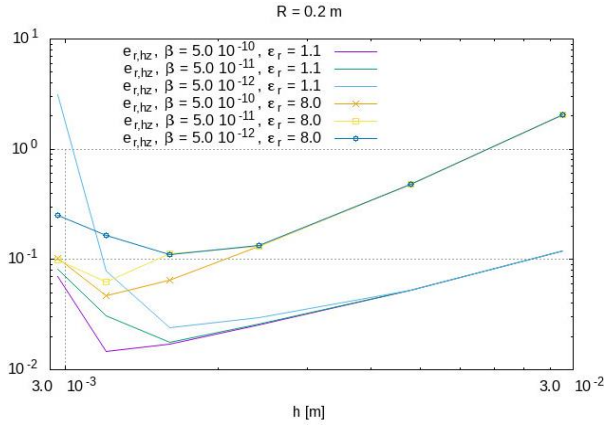


Fig. 6. Behaviour of  $e_{r,hz}$  versus  $h$  for different values of  $\beta$  and  $\epsilon_r$ . We consider  $\epsilon_r = 1.1$  and  $\epsilon_r = 8.0$  with  $\beta = 5.0 \cdot 10^{-m}$  and  $m = 10, 11, 12$ .

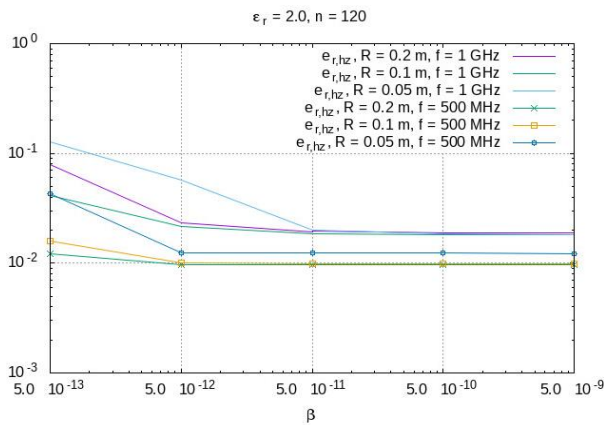


Fig. 7. Behaviour of  $e_{r,hz}$  versus  $\beta$  for different values of the scatterer radius  $R$  and of the frequency  $f$ . The values of  $\beta$  which are particularly critical for  $e_{r,hz}$  are considered. The cylinder is assumed to be made up of a material having  $\epsilon_r = 2$  at rest. The numerical solutions are computed by using a mesh with  $n = 120$ .

In Fig. 8 we plot the values of  $\frac{nn+ne}{ne} \frac{\|e_z\|}{\|e_t\|}$  versus  $\beta$ . As long as the computation of  $[e_t]$  is reasonably accurate, the value of  $\frac{nn+ne}{ne} \frac{\|e_z\|}{\|e_t\|}$  is as expected proportional to

$\beta^{-1}$ . For the problem considered here the constant of proportionality is close to 2 in case of  $\epsilon_r = 8$  and  $\epsilon_r = 2$  and close to 20 for  $\epsilon_r = 1.1$ . Thus the margin for error steadily decreases in accordance with Equation (25) as  $\beta$  decreases below  $5 \cdot 10^{-9}$  which corroborates the observed results.

The results in this subsection suggests that one must be careful with simulations involving weak bianisotropic effects. One needs to keep in mind the possible corruption of the results due to round-off errors. It may be required to use higher precision calculations to get reliable results in such instances. If one has a good estimate of the condition number, then it is possible to gauge the reliability of the result in terms of round-off error as indicated by Equation (25). However, the results that are obtained for the test case considered here reassure that one can obtain reliable solutions for a very wide span of parameters.

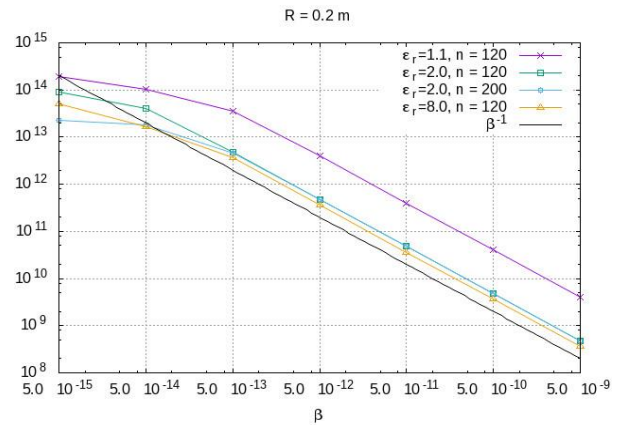


Fig. 8. Values of  $\frac{nn+ne}{ne} \frac{\|e_z\|}{\|e_t\|}$  versus  $\beta$  for different values of  $\epsilon_r$  and  $n$ . We consider  $n = 120$  with  $\epsilon_r = 1.1$ ,  $\epsilon_r = 2$  and  $\epsilon_r = 8$ . In addition, the value corresponding to  $n = 200$  with  $\epsilon_r = 2$  is also shown. A plot of  $\beta^{-1}$  provided too.

## VI. ISSUES RELATED TO NUMERICAL SOLUTION PROCEDURE

As it was already pointed out, iterative methods are very often exploited to compute the solution of the algebraic linear systems determined by electromagnetic finite element codes [19] (pp. 382, 383, 396-405). In particular, the BiCG (biconjugate gradient method) [19] (pp. 396-405) is known to be particularly efficient for time-harmonic electromagnetic problems [24] (p. 308) involving only traditional media. However, we observed that in our case, this method fails to converge for values of  $\beta$  which are not very small. This is because the structure of the matrix  $[A]$  is altered, since its submatrices  $[A_{zt}]$  and  $[A_{tz}]$  become more significant for higher  $\beta$  values. We may use some alternative iterative methods

in such cases [21], [25]. In particular, CGNE (Conjugate gradient on normal equation) is a simple alternative. However, the condition number is squared in this case resulting in slower convergence and worse round-off errors. Use of preconditioner can help improve the condition number of the system both when BiCG and CGNE are used. Simple Jacobi preconditioner was used for this purpose in the present work and the corresponding methods are denoted as BiCGJP and CGNEJP.

All the results shown in Section V were calculated by using BiCG, BiCGJP, CGNE or CGNEJP. We give a brief discussion of their performance here. If the algebraic linear system to be solved is  $[A][e] = [L]$ , as reported in Section III, we initially calculate the euclidean norm  $||[L]||$  of  $[L]$  and do not stop the iterative solver until the approximate solution  $[e]_i$  at iteration  $i$  satisfies  $||[A][e]_i - [L]|| < \delta ||[L]||$ , with  $\delta$  always equal to  $10^{-p}$ ,  $p \in \{10, \dots, 16\}$ . One should avoid using larger values of  $p$  when double-precision arithmetic is used [21] (p. 58). In order to avoid presenting unreliable results we computed them at least twice, for two consecutive values of  $p$ . When the outcomes were different we considered the next larger value of  $p$  and did not stop this process until, for two consecutive values of  $p$ , we got the same result (with a tolerance equal to 0.1%).

Independently of the reliability of the outcome, we find that the BiCGJP is able to compute the solutions for all values of  $\beta$  and  $p$  considered and all  $n \leq 80$ . For finer meshes the convergence of biconjugate iterative solvers is not guaranteed anymore. Consider, for example, some data for the test cases with  $\varepsilon_r = 2$ ,  $R = 0.2$  m and  $f = 1$  GHz. When  $n = 120$ , BiCGJP does not converge for  $\beta \geq 5 \cdot 10^{-5}$  (for this specific example the smallest residual value seems to be  $\approx 0.26$  which is by far too large to stop the iterations). BiCG fails to converge, with the same  $n$ , for  $\beta \geq 5 \cdot 10^{-3}$  (the smallest residual value is  $\approx 0.026$ ). For a mesh obtained by using  $n = 160$  BiCG (respectively, BiCGJP) does not converge for  $\beta \geq 5 \cdot 10^{-7}$  (respectively,  $\beta \geq 5 \cdot 10^{-5}$ ). When  $\beta = 5 \cdot 10^{-7}$  the smallest residual value is  $\approx 3.2 \cdot 10^{-7}$  (respectively,  $\approx 0.28$  for  $\beta = 5 \cdot 10^{-5}$ ). For the same mesh, by using  $p = 13$ , BiCGJP converges in 20214 steps (with the indicated mesh we have 308161 unknowns) for  $\beta = 5 \cdot 10^{-7}$  and in 242643 steps for  $\beta = 5 \cdot 10^{-6}$ . Finally, when  $n = 200$  we have 481201 unknowns and BiCGJP and BiCG fail to converge for  $\beta \geq 5 \cdot 10^{-7}$ , reaching a minimum residual value, for  $\beta = 5 \cdot 10^{-7}$ , of  $0.45 \cdot 10^{-5}$  and, respectively, 0.5. For this mesh, BiCGJP converges in 22956, 20001, 17834 and 13415 steps for  $\beta = 5 \cdot 10^{-m}$ , with  $m$  respectively equal to 8, 9, 10, 11 for  $p = 15$ . It is also interesting to point out that it converges in 3556 steps for  $\beta = 0$  (and  $p = 15$  as before).

From the previous considerations, one can also understand that most of our results were calculated

by using CGNE or CGNEJP. The convergence of this type of algebraic solver, however, is by far too slow, independently of the use of the preconditioner. Even though this is not a surprise [24] (p. 308), [21] (p. 18), it is instructive to report some data. For example, CGNE, for  $p = 15$  and  $n = 200$ , requires 536957 steps to converge for  $\beta = 5 \cdot 10^{-6}$  and 710410 steps for  $\beta = 0.25$  ( $\varepsilon_r = 2$ ,  $R = 0.2$  m,  $f = 1$  GHz). The results are not much better when the point Jacobi preconditioner is used. For example, with the usual values of  $\varepsilon_r$ ,  $R$  and  $f$ , for  $n = 120$  and  $\beta = 0.25$  CGNEJP converges in 220942 steps (173521 unknowns) while CGNE does the same requiring 233866 steps ( $p = 13$  in both cases). In terms of CPU time the difference is even lower (equal, more or less, to 4% on the same computer).

Thus, for small values of  $\beta$  BiCG and BiCGJP are suitable for giving fast convergence and lower round-off errors compared to CGNE and CGNEJP. The methods break down for larger values of  $\beta$  and we can use CGNE or CGNEJP which converge but at a much slower rate.

## VII. CONCLUSIONS

The accuracy of finite element results in the presence of axially moving cylinders is analyzed for the first time, to the best of authors' knowledge.

The study refers to relative and absolute errors related to two components of the electromagnetic field. The part of the results presented concerning one of the two components is new but the outcome is analogous to the one which is obtained when all media involved are motionless. The second part is related to the field component which is specifically excited by the presence of moving objects. This field component is the most difficult to be approximated. For its information content related to the motion of the objects, it could also be the most important component to be evaluated, at least for some applications.

This study has shown that finite element simulators based on double precision arithmetic could guarantee extraordinary reliability of all their outcomes. These performances suggest that the indicated simulators can be exploited and could become the reference method for astrophysics, engineering and medical applications involving media in motion.

## REFERENCES

- [1] J. G. Van Bladel, *Electromagnetic Fields*. 2nd ed., Piscataway, NJ, USA: IEEE Press, 2007.
- [2] J. H. Alwash and L. J. Qaseer, "Three-dimension finite element analysis of a helical motion induction motor," *Applied Computational Electromagnetics Society Journal*, vol. 25, no. 8, pp. 703-712, 2010.
- [3] A. M. Messiaen and P. E. Vandenplas, "High-frequency effect due to the axial drift velocity of a plasma column," *Physical Review*, vol. 149, pp.

- 131-140, September 1966.
- [4] C. Yeh, "Scattering obliquely incident microwaves by a moving plasma column," *Journal of Applied Physics*, vol. 40, no. 13, pp. 5066-5075, December 1969.
- [5] T. Shiozawa and S. Seikai, "Scattering of electromagnetic waves from an inhomogeneous magneto-plasma column moving in the axial direction," *IEEE Transactions on Antennas and Propagation*, vol. 20, no. 4, pp. 455-463, July 1972.
- [6] J. V. Parker, J. C. Nickel, and R. W. Gould, "Resonance oscillations in a hot nonuniform plasma," *Physics of Fluids*, vol. 7, no. 9, pp. 1489-1500, September 1964.
- [7] D. Censor, "Scattering of electromagnetic waves by a cylinder moving along its axis," *IEEE Transactions on Microwave Theory and Techniques*, vol. 17, no. 3, pp. 154-158, March 1969.
- [8] Y. Yan, "Mass flow measurement of bulk solids in pneumatic pipelines," *Measurement Science and Technology*, vol. 7, no. 12, pp. 1687-1706, 1996.
- [9] A. Freni, C. Mias, and R. L. Ferrari, "Finite element analysis of electromagnetic wave scattering by a cylinder moving along its axis surrounded by a longitudinal corrugated structure," *IEEE Transactions on Magnetics*, vol. 32, no. 3, pp. 874-877, May 1996.
- [10] A. Sommerfeld, *Electrodynamics*. ser. Lectures on Theoretical Physics. Academic Press, 1959.
- [11] D. K. Cheng and J.-A. Kong, "Covariant descriptions of bianisotropic media," *Proceedings of the IEEE*, vol. 56, no. 3, pp. 248-251, March 1968.
- [12] M. Brignone and M. Raffetto, "Well posedness and finite element approximability of two-dimensional time-harmonic electromagnetic problems involving non-conducting moving objects with stationary boundaries," *ESAIM: Mathematical Modelling and Numerical Analysis*, vol. 49, no. 4, pp. 1157-1192, July-August 2015.
- [13] M. M. Botha and D. B. Davidson, "Investigation of an explicit, residual-based, a posteriori error indicator for the adaptive finite element analysis of waveguide structures," *Applied Computational Electromagnetics Society Journal*, vol. 21, no. 1, pp. 63-71, 2006.
- [14] P. G. Ciarlet and J. L. Lions (Eds.), *Handbook of Numerical Analysis, vol. II, Finite Element Methods, Part I*. Amsterdam: North-Holland, 1991.
- [15] M. Pastorino and M. Raffetto, "Scattering of electromagnetic waves from a multilayer elliptic cylinder moving in the axial direction," *IEEE Transactions on Antennas and Propagation*, vol. 61, no. 9, pp. 4741-4753, September 2013.
- [16] M. Pastorino, M. Raffetto, and A. Randazzo, "Electromagnetic inverse scattering of axially moving cylindrical targets," *IEEE Transactions on Geoscience and Remote Sensing*, vol. 53, no. 3, pp. 1452-1462, March 2015.
- [17] M. Brignone, G. L. Gragnani, M. Pastorino, M. Raffetto, and A. Randazzo, "Noise limitations on the recovery of average values of velocity profiles in pipelines by simple imaging systems," *IEEE Geoscience and Remote Sensing Letters*, vol. 13, no. 9, pp. 1340-1344, September 2016.
- [18] J. D. Jackson, *Classical Electrodynamics*. 3rd ed., New York: Wiley, 1999.
- [19] J. Jin, *The Finite Element Method in Electromagnetics*. New York: John Wiley & Sons, 1993.
- [20] P. Monk, *Finite Element Methods for Maxwell's Equations*. Oxford: Oxford Science Publications, 2003.
- [21] R. Barrett, M. Berry, T. F. Chan, J. Demmel, J. Donato, J. Dongarra, V. Eijkhout, R. Pozo, C. Romine, and H. Van der Vorst, *Templates for the Solution of Linear Systems: Building Blocks for Iterative Methods*. 2nd Edition. Philadelphia, PA: SIAM, 1994.
- [22] G. Cevini, G. Oliveri, and M. Raffetto, "Further comments on the performances of finite element simulators for the solution of electromagnetic problems involving metamaterials," *Microwave and Optical Technology Letters*, vol. 48, no. 12, pp. 2524-2529, December 2006.
- [23] M. Pastorino, *Microwave Imaging*. New York: Wiley, 2010.
- [24] J. L. Volakis, A. Chatterjee, and L. C. Kempel, *Finite Element Method for Electromagnetics: Antennas, Microwave Circuits, and Scattering Applications*. Piscataway, NJ, USA: IEEE Press, 1998.
- [25] Y. F. Jing, T. Z. Huang, B. Carpentieri, and Y. Duan, "Investigating the composite step biconjugate A-orthogonal residual method for non-hermitian dense linear systems in electromagnetics," *Applied Computational Electromagnetics Society Journal*, vol. 27, no. 2, pp. 112-122, 2012.